

# A Polarimetric Survey for Dust in 47 Tucanae (NGC 104)<sup>1</sup>

Juan C. Forte

*Facultad de Cs. Astronómicas y Geofísicas, UNLP, and CONICET, Argentina*  
*e-mail: forte@fcaglp.unlp.edu.ar*

Lilia P. Bassino

*Facultad de Cs. Astronómicas y Geofísicas, UNLP, and IALP-CONICET, Argentina*

E. Irene Vega

*Instituto de Astronomía y Física del Espacio, CONICET, and Facultad de Cs. Astronómicas y Geofísicas, UNLP, Argentina*

Leonardo J. Pellizza González

*Instituto de Astronomía y Física del Espacio, CONICET, Argentina*

Sergio A. Cellone

*Facultad de Cs. Astronómicas y Geofísicas, UNLP, and IALP-CONICET, Argentina*

Mariano Méndez

*SRON National Institute for Space Research, Sorbonnelaan 2, NL-3584 CA, Utrecht, the Netherlands*

## ABSTRACT

We present linear polarization in the  $V$  band for 77 stars in the field of the globular cluster 47 Tucanae (NGC 104), and for 14 bright-star-free regions, located along an elliptical isophotal contour of the cluster, as well as  $UBVRI$  measurements for the cluster nucleus. The observations show variable foreground polarization that, once removed, leaves marginally significant polarization residuals for the non-variable bright red giants. Although these residuals are small there is, however, a systematic trend in the sense that the larger ones are seen towards the south of the cluster (in a direction opposite to that of the cluster proper motion). In contrast, most of the variable stars do show significant intrinsic polarization. The behavior of the star-free regions is similar to that of the non-variable stars and sets an upper limit to the possible existence of a global pattern of scattered (and polarized) intra-cluster light in the  $V$  band. In turn, the multicolor observations of the cluster nucleus cannot be fitted with a Serkowski law and exhibit a polarization excess both in the  $U$  and  $B$  bands. This polarization could be explained as a combination of the foreground interstellar component and another one arising in dust located in the nucleus and illuminated by a bright blue post-asymptotic star (at  $48''$  from the cluster center). An inspection of a set of archive HST WFPC2 images reveals the presence of a number of dark patches in the innermost regions of the cluster. A prominent patch (some  $5''$  by  $3''$  in size) located at  $12''$  from the cluster center and with a position angle (N to E) of  $120^\circ$ , has a slightly different polarization, compared to that of the cluster nucleus, and appears as a good candidate to be identified as a dust globule within the cluster.

*Subject headings:* Globular Clusters: Polarimetry, Dust—Globular Clusters: individual: NGC 104;  
47 Tucanae

<sup>1</sup>Based on observations made at the Complejo Astronómico El Leoncito, which is operated under agreement between CONICET and the National Universities of La Plata, Córdoba, and San Juan.

## 1. Introduction

Arguments in favor and against the presence of dust within globular clusters have been given along the years. Although an increasing volume of recent infrared observations suggests that the dust content should be very small, if any, the number of hypothesis regarding the nature of the dust particles (presumably originated by mass loss processes in luminous red giants), their spatial distribution, equilibrium temperatures, etc., render these dust mass estimates as still uncertain. A good example of this situation is depicted in the classical paper by Gillett et al. (1988) who discuss IRAS observations of the globular cluster 47 Tucanae (NGC 104) and report the existence of excess infrared emission at  $100\ \mu\text{m}$  attributed to dust thermal emission. That result can be confronted with more recent ISO observations that reach  $120\ \mu\text{m}$  (Hopwood et al. 1999), and do not confirm the presence of such excess. Both papers are illustrative of the difficulties, among others, involved in the subtraction of the stellar background (see also Knapp, Gunn, & Connolly 1995).

Among the arguments in favor of dust within globulars, and starting with the statistical approach by Roberts (1960), we can mention the multicolor photometric observations by Kanagy & Wyatt (1978) and Forte & Méndez (1988), or the polarimetry by Martin & Shawl (1981) and Forte & Méndez (1989). In turn, Auriere & Leroy (1990), disputed these results and pointed out that, in some cases, neither the photometric nor the polarimetric observations could yield an unambiguous answer to the nature of the dark patches seen in several globular clusters, i.e., if they are real dust clouds or just statistical fluctuations of the stellar distribution or, alternatively, if the dust is inside or simply along the line of sight to the cluster.

This paper presents a linear polarization survey of the globular cluster 47 Tucanae (NGC 104). Because of its high metallicity and high mass, this cluster appears as a good candidate to form and retain (at least some) dust. The structure of the survey includes three different components, namely,

1. The search for intrinsic polarization in the most luminous red giants that, due to mass loss processes, could form and eject dust par-

ticles. The integrated scattered light will be polarized only if the resulting dust shells from those processes are not spherically symmetric around the star. This kind of survey has been carried out (with negative results) by Minniti, Coyne, & Tapia (1990) and Minniti, Coyne & Clariá (1992) and, in the case of 47 Tuc itself, by Origlia et al. (1997) who, however, mention the possible detection of intrinsic polarization in some of its red variable stars.

2. The search for tangential polarization (i.e., perpendicular to the direction to the cluster center at a given position) arising in dust illuminated by the overall radiation field. The use of this effect as a diagnosis tool for dust within stellar systems was proposed originally by Jura (1978). For example, the existence of low optical depth dust distributed around the cluster center (and following some kind of radial dependence) would produce a regular pattern of the polarization  $P$ , i.e., a double wave behavior of the  $U$  and  $Q$  Stokes parameters defined as  $U = P \sin(2\theta)$  and  $Q = P \cos(2\theta)$ , with position angle on the sky. For this purpose a number of bright-star-free regions were observed following, approximately, an isophotal contour of the cluster and avoiding bright stars (no star brighter than  $V \sim 15.0$  could be seen within the diaphragm).
3. A multicolor analysis of the cluster nucleus using several aperture diaphragms ranging from  $17''$  to  $45''$  in diameter. A wavelength dependence of the polarization should show the feature of interstellar dust along the line of sight to the cluster typified by a Serkowski (1973) law. Alternatively, a deviation from that law might indicate the presence of excess polarization with a different wavelength dependence as would be expected, for example, in the case of light scattered by dust particles.

## 2. The Observations

Linear polarization observations were carried out in September or October during 1997, 1998, 1999, 2000 and 2001 runs with the 2.15 m telescope at the Complejo Astronómico El Leoncito

(San Juan, Argentina) and a rotating plate polarimeter. This instrument, is an improvement of the original designs known as MINIPOL and VATPOL (see Magalhães, Benedetti, & Roland 1984) and takes advantage of two high throughput photocells (Martínez et al. 1990). Standard stars for polarization were observed in all runs aiming at determining both the instrumental polarization (less than 0.02% in all the *UBVRI* filters) and the zero point of the polarization angle system.

Visual polarizations were measured using a 17'' diaphragm centered at the position of bright red giants, i.e., the output values correspond not only to the stars but also to the fainter stellar background within the diaphragm. No attempt was made to correct for a local background, since it varies in a strong way with position within the cluster and, instead, a blank region located 45' to the south of the cluster center was repeatedly observed during each night in order to determine the temporal variation of the sky polarization. Integration times ranged from 10 to 15 minutes per observation. The rms error of the polarization, estimated according to Magalhães et al. (1984), as a function of magnitude, can be well represented with  $\sigma P_V (\%) = 0.015V - 0.117$ , where  $V$  is the magnitude corresponding to the total brightness within the 17'' diaphragm. For the whole sample we obtain a median rms error  $\sigma P_V = \pm 0.045\%$ , that leads to a typical uncertainty of  $\sim \pm 3^\circ$  in the polarization angles. Corrections to the observed polarizations due to noise bias were estimated following Clarke & Stewart (1986) and neglected since, in the worst cases, resulted smaller than 0.01%.

The bright-star-free regions are approximately located along the isophotal contour of the cluster corresponding to a major semi-axis of 110'', i.e., some 4.6 core radii, adopting a core radius of 24'' (see, for example, Howell, Guhathakurta, & Gilliland 2000). These regions were also observed with a 17'' diaphragm and integration times of 15 min each, yielding a typical polarization error of  $\sigma P_V = \pm 0.05$ .

Polarimetry of the cluster nucleus was obtained through *UBV* (Johnson) and *RI* (Kron-Cousins) filters during the 1997 run. In this case, the observations were carried out through diaphragms with diameters of 17'', 33'', and 45'' and integration times from 5 to 15 minutes for each observation.

In total, we obtained eight integrations in the *V* and *R* bands and five for each of the remaining filters. Neutral filters were added for the *VRI* observations in order to avoid saturation due to the brightness of the cluster nucleus.

Sky polarization measurements for the bright-star-free regions and for the nucleus were also secured at the blank region 45' to the south of the cluster.

Approximate *V* magnitudes were determined for the total brightness observed through the 17'' diaphragm by means of  $V = v_i + C_V$ , where  $v_i$  is the instrumental visual magnitude (corrected by atmospheric extinction) and  $C_V = 0.19 \pm 0.05$  a constant derived by means of 19 stars included in the photometry by Lee (1977). These stars are far from the cluster center and not affected by crowding. No color term was added on the basis that most of the program stars have color indices within the color range covered by the calibrating stars.

### 3. The Observed Polarizations

#### 3.1. The Non Variable Stars

Figure 1 shows the finding chart for 53 stars (not reported as variables) located within 4' from the cluster center, and whose observed *V* polarizations are presented in Table 1 and shown on the sky in Figure 2(a). That table gives the star identification number, coordinates (J2000), the approximate *V* magnitude measured within the 17'' diaphragm, the observed linear visual polarization, associated error, and polarization angle (N to E). These data are followed by the star identification and membership probability (when available) from the proper motion study by Tucholke (1992), as well as the identification, *V* magnitudes and (*B*−*V*) colors, from Chun & Freeman (1978) and, in the last column, the heliocentric radial velocities from Mayor et al. (1983).

From the 53 stars listed in Table 1, 44 seem to be bright red giants and cluster members, according to their position in the *V* vs. (*B*−*V*) diagram. This number increases to 46 by adding one star with high membership probability from its proper motion (star 43 with no photometry available), and by including an early type post-asymptotic star labeled as BS by Lloyd Evans (1974) and UIT7 by O'Connell et al. (1997); also see Dixon, Davidsen, & Ferguson (1995). For this

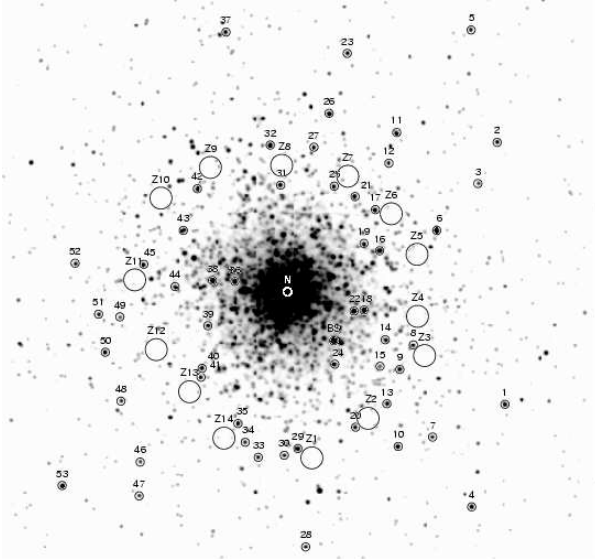


Fig. 1.— Identification chart for the observed giant stars in 47 Tuc. North is up, East to the left. The bright early post-asymptotic star is labeled as BS (see text). Larger circles correspond to the bright-star-free regions.

particular star we obtain  $P_V = 0.37\% \pm 0.02$  and  $\theta_V = 123.1^\circ$ . In turn, 39 of the observed stars have radial velocities that are consistent with membership and denote the cluster rotation (when plotted against their linear coordinates along the major axis of the cluster; see Mayor et al. (1984)).

We note that, even though six stars have low membership probability from their proper motions ( $mp$  index lower than 0.2), neither their position in the c-m diagram nor their polarization values exhibit significant differences with other stars considered as cluster members and, for this reason, were kept within the sample.

Table 2 extends the polarization observations to other 14 stars located at angular distances between  $4'$  and  $20'$  from the cluster center. Column 2 and 3 in this table give only approximate rectangular positions with respect to the cluster center (X and Y positive towards the East and North, respectively). All these stars have two color photometry given by Lee (1977) indicating that they are probable cluster members. One of them, L1427, as discussed later, seems to be associated with a long tail-like structure detected on the IRAS raster image presented by Gillett et al. (1988).

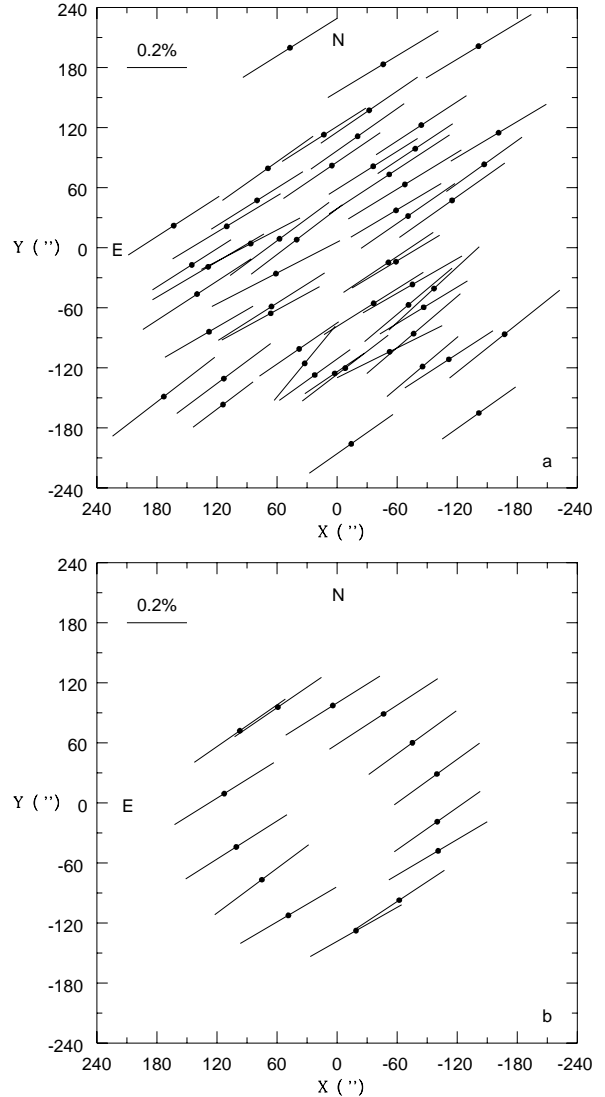


Fig. 2.— Visual polarization vectors for the 47 Tuc (non-variable) red giants projected on the sky (2-a) and for the bright-star-free regions (2-b).

### 3.2. The Variable Stars

The observed polarizations for the variable stars are given in Table 3. The identification numbers come from Sawyer-Hogg (1973). One of these objects (V4) shows discrepant values when comparing the 1997 and 1999 data; both sets are given in Table 3 as we cannot reject a possible variation of the polarization.

### 3.3. The Bright-Star-Free Regions

The polarizations corresponding to the bright-star-free regions are listed in Table 4 and displayed on the sky in Figure 2(b). That table also includes the coordinates (J2000), approximate integrated  $V$  magnitudes, and position angles on the sky measured at the cluster center (N to E).

### 3.4. The Cluster Nucleus

The  $UBVRI$  observations of the cluster nucleus are listed in Table 5. The adopted coordinates for the cluster center were (J2000)  $\alpha = 00^{\text{h}} 24^{\text{m}} 5^{\text{s}}.95$  and  $\delta = -72^{\circ} 04' 53''$ , within  $2''$  from the center coordinates estimated by Guhathakurta et al. (1992). Even though the polarizations were obtained using three different diaphragms, the  $BVRI$  values do not show a significant trend with aperture and then we only give the average values for each of these bands. The ultraviolet measures do show significant differences in polarization with aperture (see Section 7) and then the individual values for each diaphragm are given.

## 4. The Foreground Polarization

The detection of intrinsic polarization requires the removal of the foreground component arising in the interstellar dust along the line of sight to the cluster. Estimates of the color excess  $E_{(B-V)}$  produced by this dust range from 0.03 to 0.04 (see Hesser et al. 1987).

In order to map the foreground polarization on a scale of few arcmin, we first used the observations of the non-variable stars listed in Table 1. The normalized Stokes parameters for these stars were approximated by a least squares fit to two planes defined as:

$$\begin{aligned} U &= a_u X + b_u Y + C_u \\ Q &= a_q X + b_q Y + C_q \end{aligned}$$

where  $X, Y$  are the rectangular coordinates of the stars (in arcsecs) in a system with the positive  $X$  axis pointing towards the East, the positive  $Y$  axis towards the North and the origin at the cluster center. The units of the  $a$  and  $b$  coefficients are, then,  $\% \text{ arcsec}^{-1}$  and  $\%$  for the  $C$  ones. The resulting coefficients and associated errors are:  $a_u = -7.7(\pm 2.5) \times 10^{-6}$ ;  $b_u = -4.95(\pm 2.0) \times 10^{-6}$ ;  $C_u = -0.34 \pm 0.02$  and  $a_q = -1.22(\pm 1.5) \times 10^{-4}$ ;

$b_q = -2.15(\pm 0.5) \times 10^{-4}$ ;  $C_q = -0.14(\pm 0.02)$ , and show a mild trend of the  $U$  parameter with both  $X$  and  $Y$  while the  $Q$  parameter exhibits a detectable positional dependence mainly with the  $Y$  coordinate. A comparison between the polarization predicted by the plane fitting (at the position of each star) and a smooth average of the observed polarizations as a function of position angle (measured at the center of the cluster) is depicted in Figure 3. The smooth average polarizations were obtained by computing the mean  $U$  and  $Q$  values within sectors  $45^\circ$  wide and adopting a step of  $22.5^\circ$ . That figure shows that the plane fit is a good overall representation of the polarization variation within  $4'$  from the cluster center both in amplitude and angle. In turn, the  $C_u$  and  $C_q$  values lead to  $P_V = 0.37\% \pm 0.02$  and  $\theta_V = 123.8^\circ$  that is representative of the interstellar polarization at the cluster center, in very good agreement with the (unfiltered) polarimetry by Mathewson & Ford (1970), who obtain  $P = 0.36\% \pm 0.09$  and  $\theta = 123.0^\circ$ .

If a color excess of  $E_{(B-V)} = 0.04$  is adopted for the interstellar reddening towards 47 Tuc, and taking into account the relation between polarization efficiency and color excess derived by Serkowski, Mathewson, & Ford (1975),  $P_V = 9.0 E_{(B-V)}$ , the estimated polarization for the cluster center is compatible with a situation of maximum grain alignment and then maximum polarization efficiency (i.e., degree of polarization per color excess or extinction in magnitudes). We note that the IRAS calibrated  $E_{(B-V)}$  map by Schlegel, Finkbeiner, & Davis (1999) predicts a somewhat smaller color excess,  $E_{(B-V)} = 0.03$ , at the position of the 47 Tuc center. This map shows a very uniform color excess on an angular scale of  $4'$  from the cluster center, i.e., the polarization variation seems more associated with a change in polarization efficiency than with a varying foreground extinction.

The polarization behavior within  $4'$  from the cluster center can be compared with that of the stars listed in Table 2 (located between  $4'$  and  $20'$  from the center). In this case, the relatively small number of member stars, and the somewhat uneven distribution on the sky, prevent a treatment similar to that of the inner field. However, as shown in Figure 4, the behavior of  $P_V$  for stars in this sample, and that of the inner field stars,

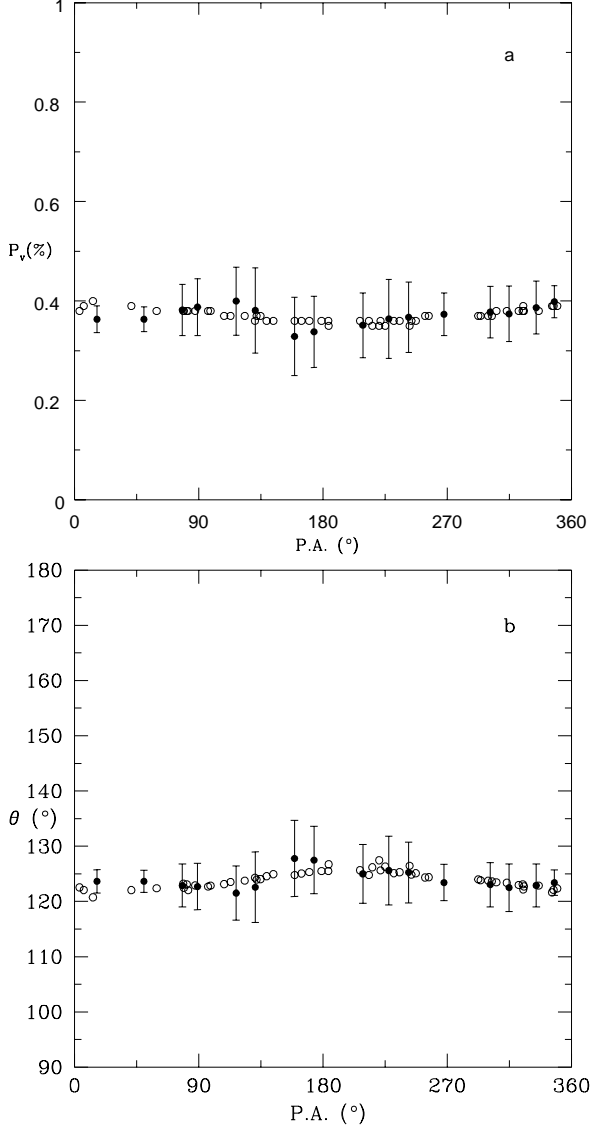


Fig. 3.— Smoothed  $P_V$  polarization (3-a) and polarization angle  $\theta_V$  (3-b) for the red giants compared with the expected polarizations obtained from the  $U$  and  $Q$  plane fittings (open circles) as a function of position angle measured at the cluster center. The bars represent the dispersion of the mean polarization values.

are compatible with an overall variation of the polarization along the N-S direction. Thus, the observed variation within  $4'$  of the cluster center does not seem a feature just connected with the cluster but, rather, a consequence of a variation of the

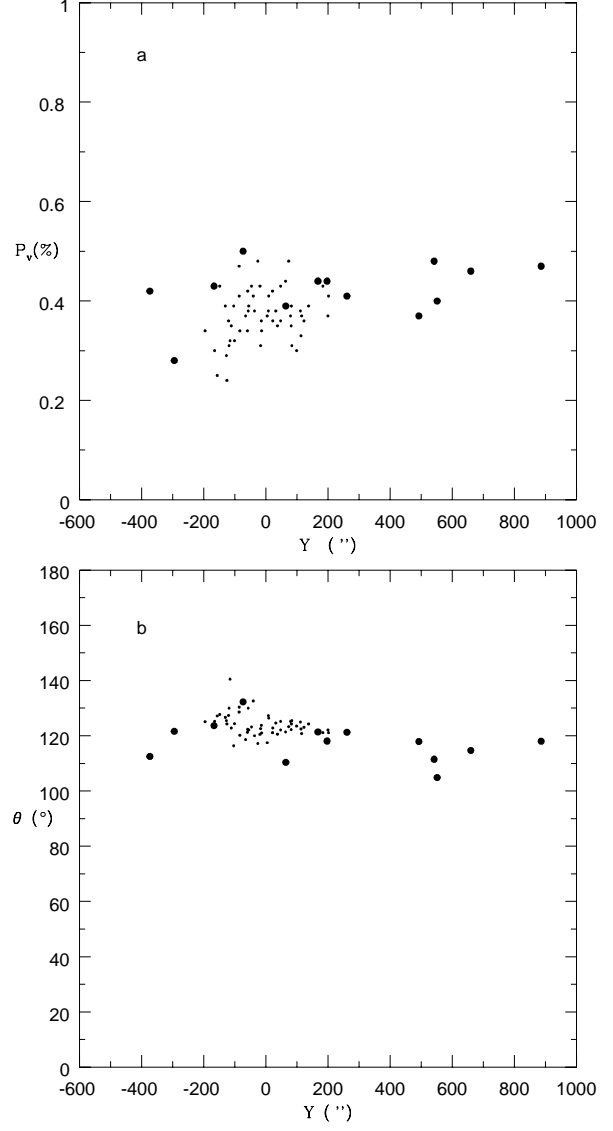


Fig. 4.— Polarization  $P_V$  vs.  $Y$  coordinate (S-N) (4-a) and polarization angle  $\theta$  vs.  $Y$  (4-b) for the outer 47 Tuc field (filled circles) and for the inner cluster field (dots).

polarization on a larger angular scale on the sky.

Figure 4 does not include the star L1421 (listed in Table 2) since, as mentioned in Section 2, this object appears associated with an elongated infrared structure and, after removing the interstellar component, shows an intrinsic polarization  $P_V = 0.38\%$  and  $\theta_V = 80.0^\circ$ .

Figure 5, in turn, shows the variation of the po-

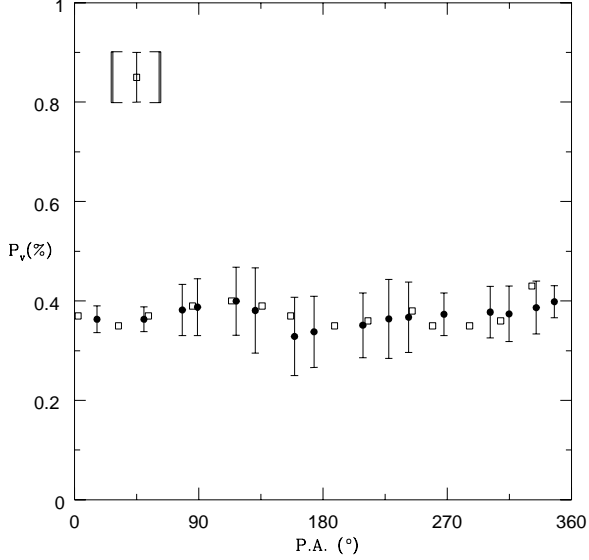


Fig. 5.— A comparison of the smoothed star polarizations with those corresponding to the bright-star-free regions (open squares) as a function of position angle. Polarization samples were taken within  $45^\circ$  sectors moved with  $22.5^\circ$  steps. The bars represent the dispersion of the mean polarization values. The bar in the upper left is representative of the errors for the bright-star-free-regions.

polarization observed in the bright-star-free regions, as a function of their position angle, compared with the smooth average polarization of the non-variable stars. The very good agreement, in this case, also lends support to the fact that most of the observed variation of the polarization is due to the foreground interstellar component.

### 5. The Residual Polarizations

The residual polarizations, after subtracting the foreground component defined by the parameters discussed in the previous section, are shown on the sky plane both for the inner field stars and for the star-free regions in Figure 6 and, on the Stokes plane, in Figure 7. The main features in these diagrams are: a) Most of the residual polarizations seem consistent with observational errors, and practically, no star exhibits values exceeding the  $3\sigma P_V$  level; b) There is no systematic angular pattern, neither for the star nor for the star-free-region polarizations.

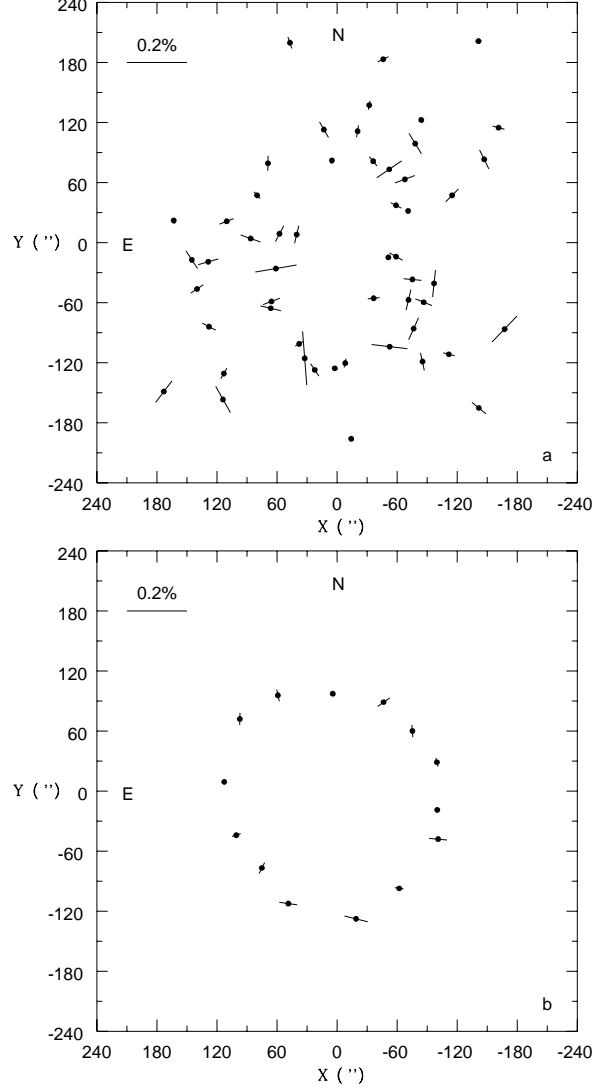


Fig. 6.— Residual polarizations (i.e., after removing the foreground interstellar component) for the red giants (6-a), and for the star-free-regions projected on the sky (6-b).

From these results we conclude that intrinsic polarizations associated with dusty shells, are not detectable in most of the non-variable stars.

Even though these residual polarizations are not large compared with the errors of the observations, a plot of these values as a function of the Y coordinate (along the N-S direction), displayed in Figure 8, shows a systematic trend in the sense that the larger polarizations are located towards



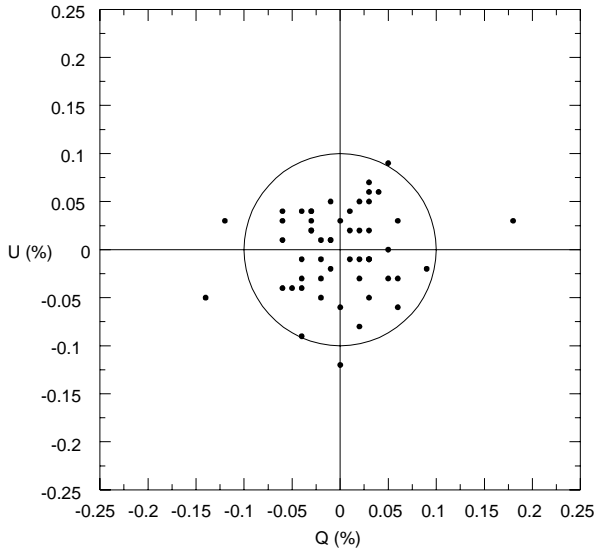


Fig. 7.—  $U$  vs.  $Q$  Stokes plane for the non variable red giants after removing the interstellar polarization. The circle has a radius set by  $2.5 \sigma P_V$ .

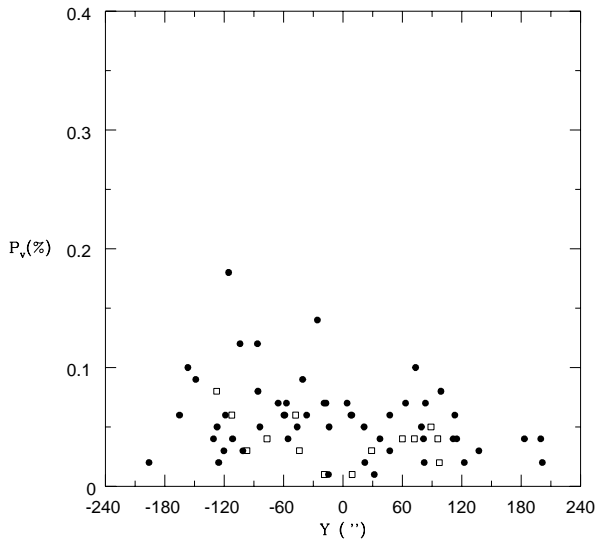


Fig. 8.— Residual polarizations for the red giants (filled circles) and for the star-free-regions (open squares) as a function of the  $Y$  coordinate (S–N). An increasing trend is seen towards the south of the cluster.

the south of the cluster center. Eight (out of nine stars) with residual polarizations at a  $2 \sigma P_V$  level or larger, appear in that position. This trend is also seen in the two southernmost star-free re-

gions (also plotted in Figure 8). Although this effect is marginal, and deserves higher precision polarimetry in order to be confirmed, it could be an indication of the presence of small amounts of scattered light. As the polarimeter aperture includes an important fraction of background light the nature of the observed polarization, i.e., if the residual polarizations are originated by the stars or by the background light, is not clear. However, as most of the bright-star-free regions do not show detectable polarization excesses, we are inclined to believe that they could arise in low optical depth dust locally illuminated (but not necessarily originated by) some stars in the southern region. In this case, and assuming that the background light within the diaphragm is only polarized by the foreground dust along the line of sight to the cluster, the residual polarizations should be increased by a factor  $10^{0.4\delta m}$ , where  $\delta m$  is the difference between the star and the total  $V$  magnitudes listed in Table 1. In the most extreme cases such a correction leads to polarization excesses as large as 0.35 %.

The fact that the proper motion of the cluster in its own LSR, as shown in Table 3 in Krockenberger & Grindlay (1995), points towards the north, may give some basis to speculate about the nature of the observed spatial asymmetry of the residual polarizations seen in the opposite direction (see the Discussion section).

## 6. The Variable Stars

The observed  $U$  and  $Q$  parameters for the group of nine red luminous variables in our sample are displayed in Figure 9. This figure also includes a circle with a  $2.5 \sigma P_V$  radius that contains, practically, all the non variable stars (also plotted). The circle is centered at the  $U$  and  $Q$  values that are representative of the interstellar polarization ( $C_u$  and  $C_q$  parameters in Section 4). Except for the variable star V10, all the remaining ones fall outside the error circle and then exhibit a significant excess or intrinsic polarization. For seven of these stars, the excess polarizations, not corrected by the background dilution effect mentioned in the preceding section, range from 0.15 % to 0.70 % and show no preferential alignments (but see the case of the comparatively highly polarized V13 below).

The fact that most of the variable stars show intrinsic polarizations agrees with a previous ten-

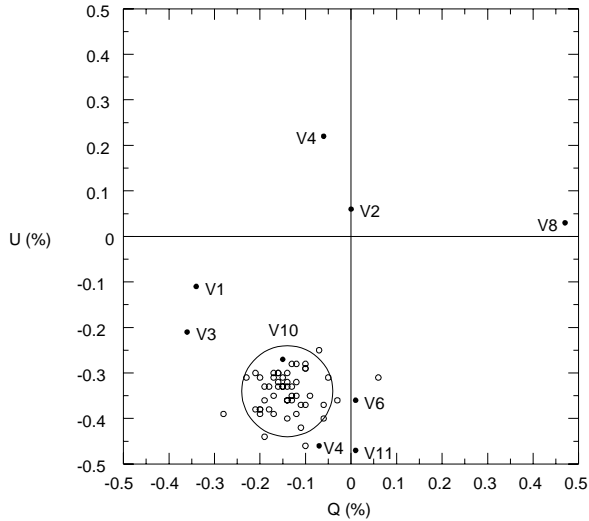


Fig. 9.— Stokes  $U$  vs.  $Q$  plane for the variable stars (filled circles). The observations corresponding to V4 are indicated in a separate way. Non variable red giants are shown as open circles. The circle has a  $2.5\sigma_{P_V}$  radius and is centered at the  $U$ ,  $Q$  values corresponding to the mean interstellar polarization along the line of sight towards the cluster. V13 falls out of the limits of the figure.

tative conclusion by Origlia et al. (1997) who point out that “...in the circumstellar environment of V1, V2, V3 and V4 we have some indication of intrinsic polarization...”. In the particular case of V1, these authors also report a detection at  $10\mu\text{m}$  attributed to dust emission. The presence of dust around V3, in turn, is supported by the high  $12\mu\text{m}$  to  $2\mu\text{m}$  flux ratio found by Ramdani & Jorissen (2001). These last authors also mention a marginal detection of dust emission around V11 based on the same flux ratio.

The variable star V13 is an interesting object (although its membership into the cluster remains to be confirmed). Its intrinsic polarization, after removing the foreground interstellar component, reaches  $P_V = 2.0 (\pm 0.15)\%$  and a polarization angle  $\theta = 123.9^\circ (\pm 3^\circ)$ , i.e., remarkably similar to that of the foreground polarization itself. This coincidence requires a further analysis in order to clarify if it happens just by chance or, alternatively, if the alignment mechanism of the foreground dust and the one that controls the circumstellar polarization in V13 are coupled in

some way. Since this last polarization is thought to arise in scattering (as supported by preliminary  $B$  band observations that show an increase of the polarization towards shorter wavelengths in V13) while the foreground dust polarization is associated with large scale magnetic fields, the physics behind that hypothetical coupling is not clear. If dust alignment by these magnetic fields is responsible for the observed polarization then, in a case of maximum polarization efficiency, a color excess  $E_{(B-V)} = 0.25$  would be required. This excess means an interstellar reddening some seven times larger than that estimated for the 47 Tuc field.

## 7. Multicolor Polarization Observations of the 47 Tucanae Nucleus

The  $UBVRI$  polarization observations of the cluster nucleus, listed in Table 5, are depicted as a function of wavelength in Figure 10. Usually, the wavelength dependence of the interstellar polarization can be adequately fit with a Serkowski (1973) curve

$$(P_\lambda/P_{\lambda_{\text{max}}}) = \exp^{-K [\ln(\lambda/\lambda_{\text{max}})]^2}, \quad (1)$$

that involves three parameters:  $\lambda_{\text{max}}$ ,  $P_{\lambda_{\text{max}}}$ , and  $K$ . Later discussions by Wilking, Lebofsky, & Rieke (1982) and Whittet et al. (1992) have shown the existence of a linear correlation between  $K$  and  $\lambda_{\text{max}}$ . In most cases, the interstellar polarization exhibits a peak with a wavelength close to  $0.55\mu\text{m}$ , which is consistent with a selective extinction ratio  $R \sim 3.0$  (Serkowski et al. 1975) a behavior that is in contrast with the fact that the nucleus of 47 Tuc shows a monotonic increase of the polarization towards shorter wavelengths. This situation cannot be considered, in principle, as an anomalous case as shown by some objects observed by Whittet et al. (1992) (see their figure 3) which have maximum polarization wavelengths as short as  $\sim 0.35\mu\text{m}$ . The assumption that the interstellar polarization curve for the 47 Tuc nucleus peaks in the  $U$  band, would imply  $K = 0.61$  according to the  $K$  vs  $\lambda_{\text{max}}$  relation given by Whittet et al. (1992). However, such a curve, normalized to  $P_V = 0.36\%$ , gives a poor representation to the observed data, as shown by Figure 10 where another fit, just considering the  $VRI$  values, is also shown. Moreover, the  $U$  band observations through the  $33''$  and  $45''$  diaphragms exhibit a significant variation in polarization amplitude and a different angle compared

with those observed for the other filters. These two features suggest that the observed polarization cannot be entirely explained as a result of an interstellar component typified by somewhat extreme values of  $K$  and  $\lambda_{\max}$ .

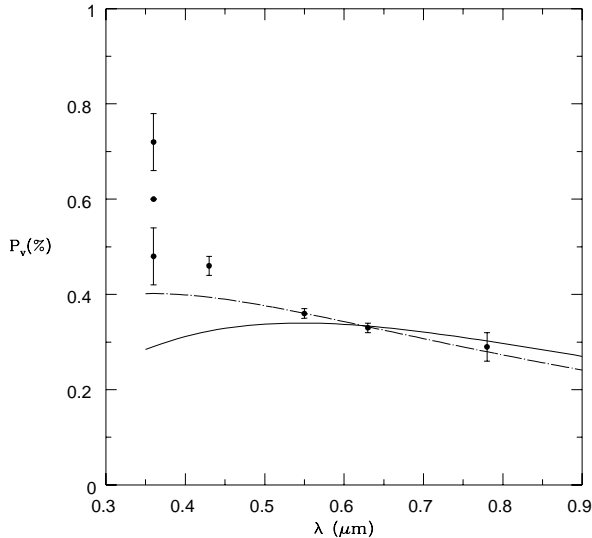


Fig. 10.— Linear polarization observed in the 47 Tuc nucleus as a function of wavelength of the *UBVRI* bands. Three different values are given for the *U* filter corresponding to the 33'' and 45'' diaphragms and to their average. The lines correspond to two different Serkowski law fits with  $\lambda_{\max}$  of 0.55  $\mu\text{m}$  (solid line) and 0.36  $\mu\text{m}$  (dot-line).

We note that the observed visual polarization for the nucleus agrees, within the errors, with the estimated foreground polarization discussed in Section 3 then suggesting that the excess polarization in the *V* band, if any, is very small.

## 8. A Tentative Explanation for the Excess Polarization in the 47 Tuc Nucleus

The bright (and blue) post-asymptotic star referred as BS or UIT7 (see subsection 2.1) is located some 48'' from the cluster center and appears as a suitable candidate to be considered as the origin of the excess polarization in the nucleus for two reasons:

a) The angle of the excess polarization, after removing the ultraviolet interstellar polarization expected from a Serkowski curve, is close to “tangential” (i.e., perpendicular to the line joining the

star and the cluster center, see below) as expected if some dust in the nuclear region were asymmetrically illuminated by the star; and b) The ratio of the star to nucleus flux, as a function of wavelength, increases in a steep way towards the ultraviolet then decreasing the dilution effect produced by the light of the nucleus within a given aperture. This effect would be reflected, as observed, by an increase of the excess polarization in *U* and to a lesser extent at longer wavelengths, where that flux ratio decreases.

We quantify this polarization excess first, by adopting the average of the polarization measures through the 33'' and 45'' diaphragms,  $P_U = 0.60\%$  and  $\theta = 117.9^\circ$  and second, by removing the ultraviolet interstellar polarization. For this component, a maximum polarization wavelength of 0.36  $\mu\text{m}$  (from Figure 10) or 0.55  $\mu\text{m}$  (compatible with a more “normal” behavior), with  $P_V = 0.36\%$  and  $\theta_V = 123.8^\circ$ , leads to an excess polarization in the *U* band of 0.23 % or 0.30 %, with angles of  $\theta_U = 118.9^\circ$  and  $\theta_U = 113.7^\circ$  respectively. These polarization angles lie within less than  $20^\circ$  from the angle of the direction perpendicular to the line joining the star and the cluster nucleus ( $\sim 132^\circ$ ), that is, the polarization angle expected in the case that dust were effectively illuminated by the post-asymptotic star.

A quantitative estimate of the dust optical depth required to originate such excess polarization requires:

a) The knowledge of the spectral energy distributions both for the star and the cluster nucleus. The spectral type of UIT7 is B8III, with an apparent visual magnitude  $V = 10.73$  according to table 1 in O’Connell et al. (1997), implying a temperature  $T = 13450^\circ\text{K}$  and intrinsic colors  $(U-B)_0 = -0.44$  and  $(B-V)_0 = -0.14$  (from Cramer 1984). Alternatively, Dixon et al. (1995) obtain a considerably lower temperature,  $T = 10500^\circ\text{K}$  corresponding to  $(U-B)_0 = -0.20$  and  $(B-V)_0 = -0.01$  (Flower 1996). As a compromise we then take the average of these indices,  $(U-B)_0 = -0.32$  and  $(B-V)_0 = -0.08$  as representative for the intrinsic colors of UIT7. In turn, adopting a color excess  $E_{(B-V)} = 0.04$  towards the cluster and a selective extinction ratio  $R = 3.0$ , lead to interstellar extinction corrected magnitudes  $U_0 = 10.21$ ,  $B_0 = 10.53$  and  $V_0 = 10.61$  for the star.

For the nucleus we adopted the reddening corrected colors given by Reed, Hesser, & Shawl (1988),  $(U-B)_0 = 0.31$ ,  $(B-V)_0 = 0.82$ . Within an aperture of  $33''$  we obtain  $V \sim 7.50$  and then  $U_0 = 8.51$ ,  $B_0 = 8.20$  and  $V_0 = 7.38$ .

A comparison of the magnitudes of the star and the nucleus shows a rapid increase of the relative brightness of UIT7 towards short wavelengths, a fact that is dramatically shown by figure 1 in O’Connell et al. (1997), where the far ultraviolet luminosity of the star exceeds the integrated brightness of the cluster within the visual half light radius ( $174''$ ).

b) The adoption of a relative geometry involving the cluster nucleus, the star and the observer. The star UIT7 appears at a projected distance on the sky of  $48''$  from the cluster center. As we have no indication about the relative position of the star and the cluster nucleus along the line of sight, we leave this quantity as a free parameter in our calculation.

c) The adoption of parameters for the dust grains such as size, albedo and phase function. The fact that the excess polarization increases rapidly towards the ultraviolet, and favors a  $\lambda^{-4}$  type of dependence rather than a  $\lambda^{-1}$  law that characterizes “normal” interstellar grains, indicates that the dust scatterers might be small compared to the light wavelength. As a first approach, we then adopt highly reflective particles (i.e., unity albedo) and a Rayleigh-like phase function.

d) The size, spatial dust distribution and optical depth of the cloud. The behavior of the ultraviolet polarization, that increases from the  $17''$  diaphragm towards a maximum at  $33''$  and then decreases at  $45''$ , suggests that most of the polarization arises from within the second aperture and then we adopt an indicative cloud radius of  $16.5''$  (on the sky). The spatial dust density was represented with a function consistent with a King profile with  $r_c = 24''$ , truncated at the indicative radius mentioned above, and an optical depth (through the whole cloud diameter)  $\tau_U = 0.5$ . This value corresponds to a weighted optical depth of  $\sim 0.3$  for the whole cloud that may be somewhat large for an optically thin approach and would require depolarization corrections in a more rigorous model.

Figure 11 depicts the results, obtained with all

the mentioned assumptions, for the ratio of scattered light, arising in the illuminating star UIT7, to that of the integrated stellar light of the nucleus in the UBV bands, as a function of the “depth” coordinate, i.e., the position of the star along the line of sight in core radius units (11-a) and the resulting polarization from a single scattering approach, (and equations from Van de Hulst 1967) (11-b).

This figure indicates that the order of the observed excess polarization can be originated by a relatively low optical depth dust cloud centered at the cluster nucleus and illuminated by the star UIT7. We note that, if this cloud is mixed with the stars and also illuminated by the cluster radiation field, its effect on the integrated cluster light profile will be considerably decreased. The adoption of models like those discussed by Witt, Thronson, & Capuano (1992) show that the central profile brightness would be dimmed between 0.16 and 0.25 magnitudes in the  $U$  band (for an isotropic scattering or a Henyey-Greenstein phase function typified by an anisotropy factor  $g = 0.7$ ) and less than 0.1 magnitudes in the  $V$  band.

The estimate of the mass associated with such a cloud is dependent on the nature of the dust grains. Following Kanagy & Wyatt (1978) and adopting a cloud radius of 0.36 parsecs, corresponding to an angular radius of  $16.5''$  at a distance of 4.7 kpc (from Hesser et al. 1987):

$$M_d = 0.18 \rho(\tau) (1/Q) (r_g) M_\odot \quad (2)$$

where  $\tau$  is the average optical depth of the spherical cloud,  $\rho$  is the density (in  $\text{g cm}^{-3}$ ) of a dust grain;  $Q$ , its extinction efficiency ; and,  $r_g$  its radius in microns. For example, the adoption of astronomical silicate grains (Draine & Lee 1984) with radii in the order of a few hundred Å and  $\tau_U = 0.3$ , leads to a total dust mass of  $\sim 0.05 M_\odot$ . This mass is well above the estimates coming from far infrared observations (see the Discussion Section) and includes the uncertainty connected with the fact that interstellar grains may not be an adequate approximation to circumstellar dust (if this is the origin of the dust particles producing polarization).

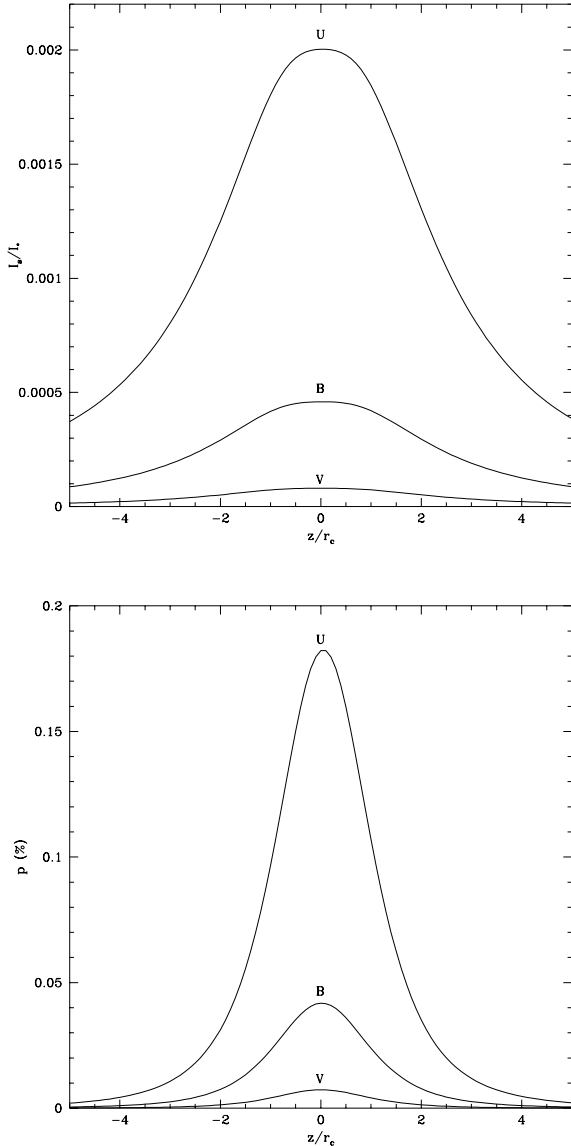


Fig. 11.— Star (UIT7) to nucleus ( $33''$  diaphragm) flux ratio in the *UBV* bands (11-a) and resulting polarization due to an spherical dust cloud at the cluster nucleus with  $\tau_U = 0.5$ , (11-b) as a function of the coordinate along the line of sight (in core radius units) and assuming Rayleigh scattering.

## 9. Cloud Candidates in the 47 Tuc Nuclear Region

An inspection of HST archive multicolor images show the presence of several dark patches within

$30''$  from the cluster nucleus. One of these patches, that exhibits a triangular shape ( $5'' \times 3''$ ), appears at  $12''$  from the cluster center and at a position angle of  $120^\circ$ . Two polarimetric measures were obtained at the position of this dark patch through a  $5''$  aperture diaphragm during the 2000 and 2001 runs. These observations were made with the *V* filter, and integration times of 300 secs each, yielding  $P_V = 0.42 \pm 0.02\%$  and  $\theta = 123.2^\circ \pm 2$ . This polarization is larger, by some 20 %, compared to that of the nucleus and suggests the existence of excess polarization associated with the dark patch. We note that the geometric shape of the patch is not matched by that of the circular diaphragm. For this reason, a relatively large amount of light coming from its peripheral regions may produce a dilution effect on the intrinsic polarization eventually arising in the dark patch itself.

## 10. Discussion

The analysis of the visual polarization of both the non-variable giant stars and of the bright-star-free regions within  $4'$  from the cluster center shows a variation that can be attributed to the foreground dust along the line of sight to 47 Tuc. This variation is consistent with the polarizations observed on a larger angular scale, i.e., stars between  $4'$  and  $20'$  from the center. An inspection of the  $E_{(B-V)}$  IRAS calibrated map (Schlegel et al. 1999) over the same region, however, does not exhibit a systematic change of reddening indicating that the observed polarization trend is more likely produced by a variation of the foreground polarization efficiency rather than by a variable optical depth of the foreground interstellar dust.

After a vectorial removal of the foreground polarization most of the residual values corresponding to the non variable stars are small, indicating that they are probably reflecting just the observing errors. However, there remains a detectable trend in the sense that the larger residuals are seen towards the south of the cluster, a direction that is opposite to that of the cluster proper motion. Krockenberger & Grindlay (1995) have suggested that the X-ray structure observed around 47 Tuc could be originated by the cluster motion and the interaction of its gas with the hot galactic halo. The same mechanism, i.e. ram pressure on dust grains, may lead to the formation

of a tail-like structure or a preferential direction along which dust grains leave the cluster (Pellizza González, Forte, & Carpintero 2002). The spatial velocity components of 47 Tucanae given in table 3 of Krockenberger & Grindlay (1995), based on absolute proper motions derived by Tucholke (1992) and Cudworth & Hanson (1993), indicate that such a tail would be located towards the south of the cluster and receding from the sky plane with an angle of about  $55^\circ$ . The lack of a regular pattern of the residual polarizations observed in some stars located towards the south of the cluster center might be explained as a consequence of optically thin dust locally illuminated by the stars themselves, or combined with back-scattering of the cluster radiation as a whole. Back-scattering properties for galactic cirrus have been discussed, for example, by Jakobsen, de Vries, & Paresce (1987). This possibility is also worth of further analysis given the existence of a diffuse far-ultraviolet background, detected on UIT observations by O’Connell et al. (1997), which has a spatial scale length that is significantly different from that of the 47 Tuc stars. The dust scattering explanation was considered by these last authors and, in principle, ruled out due to the large dust mass required if “canonical” dust grains were present and mixed with the stars.

Another argument that may also support the existence of a tail-like structure comes from the appearance of the elongated structure detected on IRAS 12  $\mu\text{m}$  raster images of the central regions of 47 Tuc by Gillett et al. (1988) (see their Figure 1-b). This detection would imply relatively large dust equilibrium temperatures for an extended source. However, other radiation mechanisms, as for example, very small particles transiently heated by absorption of single photons (Sellgren, Werner, & Dinerstein 1983), may provide an explanation consistent with the polarimetric results discussed in Section 8 that also favor the presence of small particles.

There are other elongated or cirrus-like structures in the IRAS image. As mentioned before, one of these features appears connected with the red giant L1421. Gillett et al. (1988) point out that there is no compelling evidence of the connection of this high temperature structure ( $T = 40^\circ\text{ K}$ ) with the cluster. However, the detection of intrinsic polarization in L1421 (see Section 4), a

likely cluster member, suggests that this star is illuminating the elongated cloud. Furthermore, the spatial orientation of this tail-like structure is well aligned with the direction of the spatial proper motion of the cluster, corrected for the peculiar motion of the sun and galactic rotation, based on the proper motion study by Cudworth & Hanson (1993), see Table 3 in (Krockenberger & Grindlay 1995).

In contrast with the bright non-variable red giants, almost all the observed variable stars show significant polarization excesses, a result consistent with those obtained by other authors and in the same direction of arguments already given by Frogel & Elias (1988) in the sense that dust formation and mass loss driven by stellar pulsations are connected. In any case, and according to the very low mass loss rates obtained by Ramdani & Jorissen (2001), who also point out the lack of dust enshrouded stars in 47 Tuc, the variable stars do not appear as an important source for dust injection (and replenishment) into the cluster environment.

In turn, the multicolor polarization observations of the cluster nucleus do not show a detectable polarization maximum within the *UBVRI* wavelength range and, instead, display a smooth increase towards the *U* band. This trend cannot be matched with a Serkowski law, even if we assume rather extreme assumptions about  $\lambda_{\text{max}}$  and of the *K* parameters that would imply values of the total to selective extinction ratio as low as  $R = 2.0$  or less. Besides, the fact that the *U* polarization exhibits significant changes with diaphragm aperture, and also a different polarization angle, rather suggest that the observed behavior could be a combination of the foreground interstellar polarization and of other polarizing source that becomes more evident towards short wavelengths. The blue post-asymptotic star known as BS or UIT7 may give an adequate explanation if this object is in fact illuminating some dust located in the cluster nucleus. Other possible origin, such as intrinsic polarization associated with the atmospheres of giant stars within the 47 Tuc nuclear region can be ruled out as their ultraviolet magnitudes, around  $U=16$  to  $16.5$ , are some eight magnitudes fainter than the integrated brightness of the nucleus within the  $33''$  diaphragm.

The detection of dust within the nuclear region of another metal rich globular, NGC 6356,

has been reported by Hopwood et al. (1998) on the basis of observations carried out with 850  $\mu\text{m}$  arrays. However, ISO observations of 47 Tuc itself (Hopwood et al. 1999), set a very low upper limit for the dust mass (assuming silicate or amorphous carbon grains). In fact, the peak emission at 120  $\mu\text{m}$  is offset from the cluster center by  $\sim 165''$  and a position angle of  $118^\circ$  (see figure 2 in that paper). This position angle is bracketed by those corresponding to the bright-star-free regions Z12 and Z13 (although they are closer to the cluster center). An analysis of the integrated brightness of these regions, listed in Table 4, as a function of position angle, shows that there is an overall decrease of the cluster surface brightness in that sector (including Z14 and Z1) that, in the average, are 0.5 mag. fainter than the mean defined by all the regions. This obscuration may arise in the same dust that reaches a flux of  $\sim 35 \text{ MJy sr}^{-1}$  in the ISO map. The fact that this is probably a small angular scale structure is suggested by the lack of a similar feature in the lower resolution IRAS maps.

The origin of the disagreement between the ISO results, that suggest that the nucleus is practically free of dust, and those coming from the polarimetric results presented in this paper, remains unclear. A preliminary hypothesis assumes that the particles that produce polarization (in the cluster nucleus) and those that may give rise to the 120  $\mu\text{m}$  emission (at the offset position) have markedly different physical properties. The environmental conditions of these particles may indeed be very different in terms, for example, of the ionized gas density (Freire et al. 2001) and its effect on the grain survivability.

High precision color-magnitude diagrams (e.g., based on multicolor HST images) of individual stars may provide a good test about the presence of dust although, up to now, the published photometric results are still somewhat noisy to reach definite conclusions. A dust cloud optical depth  $\tau_U = 0.5$  would imply a maximum blue extinction  $A_B$  ranging from 0.4 to 0.2 magnitudes and a color excess  $E(U - V)$  between 0.18 and 0.41 (for a  $\lambda^{-1}$  or a  $\lambda^{-4}$  wavelength extinction dependence, respectively). These values are compatible with the red envelope of the  $B$  vs.  $(U - V)$  color magnitude diagram presented by Howell et al. (2000) for stars within  $21.54''$  from the cluster center.

A multicolor photometric program is currently under way (Faifer & Forte 2002), and focused on a number of dark patches that might be identified as knotty dust clouds with sizes smaller than 0.1 parsecs inside a more diffuse dusty environment in the 47 Tuc nuclear region.

The authors acknowledge the work of the CASLEO staff in developing the polarimeter and also their enthusiastic help during the several observing runs invested in this paper. Useful remarks by an anonymous referee are appreciated. This work was partially funded by CONICET and the Agencia Nacional de Promoción Científica y Técnica de la Rep. Argentina.

## REFERENCES

- Auriere, M., & Leroy, J. L. 1990, *A&A*, 234, 164
- Chun, M. S., & Freeman, K. C. 1978, *AJ*, 83, 376
- Cramer, N. 1984, *A&A*, 132, 283
- Clarke, D. & Stewart, B.G. *Vistas Astron.*, 29, 27.
- Cudworth, K. M., & Hanson, R. B. 1993, *AJ*, 105, 168
- Dixon, W. V. D., Davidsen, A. F., & Ferguson, H. C. 1995, *ApJ*, 454, L47
- Draine, B.T., & Lee, H.M. 1984, *ApJS*, 285, 89
- Faifer, F., & Forte, J. C. 2002, in prep.
- Flower, P. J. 1996, *ApJ*, 469, 355
- Forte, J. C., & Méndez, M. 1988, *AJ*, 95, 500
- Forte, J. C., & Méndez, M. 1989, *ApJ*, 345, 222
- Freire, P. C., Kramer, M., Lyne, A. G., Camilo, F., Manchester, R. N., & D'amico, N. D. 2001, *ApJ*, 557, 105
- Frogel, J. A., & Elias, J. H. 1988, *ApJ*, 324, 823
- Gillett, F. C., de Jong, T., Neugebauer, G., Rice, W. L., & Emerson, J. P. 1988 *AJ*, 96, 116
- Guhathakurta, P., Yanny, B., Schneider, D. P., & Bahcall, J. N. 1992, *AJ*, 104, 1790
- Hesser, J. E., Harris, W. E., VandenBerg, D. A., Allwright, J. W. B., Shott, P., & Stetson, P. B. 1987, *PASP*, 99, 739

- Hopwood, M. E. L., Evans, A., Penny, A., Eyres, S. P. S. 1998, MNRAS, 301, L30
- Hopwood, M. E. L., Eyres, S. P. S., Evans, A., Penny, A. & Odenkirchen, M. 1999, A&A, 350, 49
- Howell, J. H., Guhathakurta, P., & Gilliland, R. L. 2000, PASP, 112, 1200
- Jakobsen, P., de Vries, J. S., & Paresce, F. 1987, A&A, 183, 335
- Jura, M. 1978, ApJ, 223, 421
- Kanagy, S. P., & Wyatt, S. P. 1978, AJ, 83, 779
- Knapp, G. R., Gunn, J. E., & Connolly, A. J. 1995, ApJ, 448, 195
- Krockenberger, M., & Grindlay, J. E. 1995, ApJ, 451 200
- Lee, S.-W. 1977, A&A, 27, 381
- Lloyd Evans, T. 1974, MNRAS, 167, 393
- Magalhães, A. M., Benedetti, E., & Roland, E. H. 1984, PASP, 96, 383
- Martin, P. G., & Shawl, S. J. 1981, ApJ, 251, 108
- Martínez, E., Aballay, J. L., Marín, A., & Ruardes, H. 1990, Bol. Asoc. Arg. de Astronomía, 36, 342
- Mathewson, D. S., & Ford, V. L. 1970, MmRAS, 74, 139
- Mayor, M., et al. 1983, A&AS, 54, 495
- Mayor, M., et al. 1984, A&A, 134, 118
- Minniti, D., Coyne, G. V. & Clariá, J. J. 1992, AJ, 103, 871
- Minniti, D., Coyne, G. V., & Tapia, S. 1990, A&A, 236, 371
- O’Connell, R. W., et al. 1997, AJ, 114, 1982
- Origlia, L., Scaltriti, F., Anderlucci, E., Ferraro, F. R., & Fusi Pecci, F. 1997, MNRAS, 292, 753
- Pellizza, L., Forte, J. C., & Carpintero, D. 2002, in prep.
- Ramdani, A., & Jorissen, A. 2001, A&A, 372, 85
- Reed, B. C., Hesser, J. E., & Shawl, S. J. 1988, PASP, 100, 545
- Roberts, M. S. 1960, AJ, 65, 457
- Sawyer-Hogg, H. 1973, Publ. DDO 3, No 6
- Schlegel, D. J., Finkbeiner, D. P., & Davis, M. 1998 ApJ, 500, 525
- Sellgren, K., Werner, M. W., & Dinerstein, H. L. 1983, ApJ, 271, L13
- Serkowski, K. 1973, in Proc. IAU Symposium No 52, Interstellar Dust and Related Topics, eds. J. M. Greenberg, & H. C. van de Hulst (Dordrecht: Reidel), 145
- Serkowski, K., Mathewson, D. S., & Ford, V. L. 1975, ApJ, 196, 261
- Tucholke, H. J. 1992, A&AS, 93, 293
- van de Hulst, H. C. 1967, in Light Scattering by Small Particles, Dover Inc. 1981
- Whittet, D. C. B., Martin, P. G., Hough, J. H., Rouse, M. F., Bailey, J. A., & Axon, D. J. 1992, ApJ, 386, 562
- Willing, B. A., Lebofsky, M. J., & Rieke, G. H. 1982, AJ, 87, 695
- Witt, A. N., Thronson, H. A., & Capuano, J. M. 1992, ApJ, 393, 611



TABLE 1  
VISUAL POLARIZATIONS FOR BRIGHT GIANT STARS IN 47 TUC

N	$\alpha$ (J2000) hs : min : s	$\delta$ (J2000) ° : ' : ''	$V_{17}''$ mag	$P_V$ %	$\theta_V$ °	T <sup>a</sup>	mp <sup>b</sup>	CF <sup>c</sup>	$V$ mag	$B-V$ mag	R.V. km/s
1	00:23:29.4	-72:06:20	11.27	$0.47 \pm 0.05$	128.6	1175	98.3	E175	11.63	1.86	-4.4
2	00:23:30.9	-72:02:57	11.64	$0.37 \pm 0.06$	120.8	1191	96.9	E275	12.06	1.48	-27.9
3	00:23:34.1	-72:03:29	12.02	$0.31 \pm 0.06$	125.5	1225 <sup>d</sup>	96.5	E270	12.87	1.27	-35.8
4	00:23:35.0	-72:07:39	11.43	$0.30 \pm 0.05$	125.2	...	...	E97	11.73	1.74	-10.1
5	00:23:35.3	-72:01:30	11.67	$0.41 \pm 0.06$	121.1	1243	23.7	E323	12.12	1.51	-11.5
6	00:23:40.9	-72:04:05	10.62	$0.43 \pm 0.04$	125.2	...	...	-	...	...	...
7	00:23:41.6	-72:06:45	11.16	$0.35 \pm 0.05$	122.8	1320	0	E90	12.32	1.40	-10.3
8	00:23:44.8	-72:05:34	11.61	$0.41 \pm 0.06$	132.6	...	...	F111	12.22	1.37	+1.6
9	00:23:47.1	-72:05:53	10.99	$0.34 \pm 0.05$	121.3	...	...	F86	12.03	1.49	-6.0
10	00:23:47.3	-72:06:53	11.31	$0.31 \pm 0.05$	130.0	...	...	E83	12.08	1.58	-22.3
11	00:23:47.7	-72:02:49	11.15	$0.36 \pm 0.05$	123.1	1379	0	E304	11.69	1.82	-27.8
12	00:23:49.0	-72:03:13	11.42	$0.30 \pm 0.06$	123.5	...	...	F218	12.13	1.49	-13.0
13	00:23:49.3	-72:06:20	11.24	$0.41 \pm 0.05$	130.4	1390	98.3	F66	12.00	1.50	-8.3
14	00:23:49.5	-72:05:30	11.05	$0.38 \pm 0.05$	120.0	...	...	F106	12.07	1.50	-5.6
15	00:23:50.4	-72:05:51	11.16	$0.38 \pm 0.06$	130.0	...	...	F89	12.21	1.69	-13.5
16	00:23:50.5	-72:04:21	10.45	$0.38 \pm 0.04$	124.6	...	...	F188	11.48	2.28	-26.8
17	00:23:51.2	-72:03:49	10.82	$0.44 \pm 0.04$	121.4	...	...	F203	11.70	1.77	-7.7
18	00:23:53.1	-72:05:07	10.11	$0.34 \pm 0.03$	121.0	...	...	...	...	...	...
19	00:23:53.1	-72:04:15	10.56	$0.35 \pm 0.04$	120.6	...	...	F193	11.62	1.86	-29.1
20	00:23:54.5	-72:06:38	11.29	$0.39 \pm 0.05$	116.4	...	...	F60	12.34	1.37	-14.0
21	00:23:54.6	-72:03:39	10.94	$0.48 \pm 0.05$	123.3	...	...	F229	11.71	1.76	-31.4
22	00:23:54.8	-72:05:08	10.97	$0.36 \pm 0.05$	123.8	...	...	...	...	...	...
23	00:23:56.0	-72:01:48	11.57	$0.43 \pm 0.06$	121.1	...	...	E354	12.44	1.35	-14.9
24	00:23:58.0	-72:05:49	10.64	$0.39 \pm 0.05$	122.0	...	...	...	...	...	...
25	00:23:58.1	-72:03:31	10.97	$0.35 \pm 0.05$	122.2	...	...	F260	11.74	1.61	-24.4
26	00:23:59.0	-72:02:35	11.27	$0.39 \pm 0.05$	124.3	1480	98.3	E370	11.64	1.94	10.3
27	00:24:01.5	-72:03:01	11.36	$0.38 \pm 0.05$	125.0	...	...	F276	12.03	1.50	-29.9
28	00:24:02.9	-72:08:11	11.66	$0.34 \pm 0.06$	125.1	...	...	E44	12.20	1.43	-14.4
29	00:24:04.2	-72:06:55	10.95	$0.36 \pm 0.05$	127.4	...	...	F1	11.90	1.51	-25.5
30	00:24:06.5	-72:07:00	12.30	$0.24 \pm 0.06$	124.2	...	...	F588	12.34	1.37	-22.5
31	00:24:07.1	-72:03:30	10.71	$0.39 \pm 0.05$	124.3	...	...	F290	11.86	1.62	-26.7
32	00:24:08.8	-72:02:59	10.95	$0.33 \pm 0.05$	122.5	...	...	F305	11.53	1.95	-25.3
33	00:24:10.8	-72:07:01	12.00	$0.29 \pm 0.06$	125.5	...	...	F563	12.60	1.28	...
34	00:24:13.0	-72:06:50	12.25	$0.32 \pm 0.06$	140.5	...	...	F561	12.87	1.15	...
35	00:24:14.3	-72:06:35	11.94	$0.32 \pm 0.06$	124.4	...	...	F553	12.19	1.29	-9.2
36	00:24:14.8	-72:04:45	10.50	$0.38 \pm 0.04$	127.3	...	...	...	...	...	...
37	00:24:16.2	-72:01:32	11.45	$0.37 \pm 0.06$	122.1	...	...	E397	12	1.91	-20.3
38	00:24:18.5	-72:04:44	10.11	$0.41 \pm 0.03$	126.4	...	...	...	...	...	...
39	00:24:19.3	-72:05:19	11.20	$0.48 \pm 0.05$	117.2	...	...	F478	11.93	1.58	-36.2
40	00:24:20.3	-72:05:52	11.08	$0.42 \pm 0.05$	122.3	...	...	F490	12.08	1.44	-19.8
41	00:24:20.5	-72:05:59	11.63	$0.37 \pm 0.06$	118.6	...	...	F507	12.17	1.42	-9.6

TABLE 1—*Continued*

N	$\alpha$ (J2000) hs : min : s	$\delta$ (J2000) ° : ' : ''	$V_{17''}$ mag	$P_V$ %	$\theta_V$ °	T <sup>a</sup>	mp <sup>b</sup>	CF <sup>c</sup>	$V$ mag	$B-V$ mag	R.V. km/s
42	00:24:21.0	−72:03:33	11.16	$0.37 \pm 0.05$	125.2	...	...	F338	11.80	1.70	...
43	00:24:23.4	−72:04:06	10.92	$0.36 \pm 0.05$	122.1	1700	98.4	...	...	...	...
44	00:24:24.8	−72:04:49	10.87	$0.37 \pm 0.05$	117.5	...	...	F429	11.80	1.68	−24.5
45	00:24:30.0	−72:04:32	11.55	$0.42 \pm 0.06$	121.1	1774	56.6	F400	11.82	1.69	−27.8
46	00:24:30.7	−72:07:05	12.16	$0.39 \pm 0.06$	126.7	...	...	E630	12.88	1.20	...
47	00:24:30.9	−72:07:31	12.65	$0.25 \pm 0.07$	127.2	...	...	E629	12.86	1.10	...
48	00:24:33.9	−72:06:18	11.92	$0.34 \pm 0.06$	120.2	1816	15.4	E587	12.77	1.27	−12.2
49	00:24:34.1	−72:05:13	12.07	$0.43 \pm 0.06$	120.5	...	...	F445	13.05	1.20	...
50	00:24:36.5	−72:05:40	11.34	$0.43 \pm 0.05$	123.2	...	...	E582	11.95	1.62	−26.5
51	00:24:37.6	−72:05:11	11.73	$0.31 \pm 0.06$	122.6	1862	0	E647	12.78	1.10	...
52	00:24:41.6	−72:04:31	11.76	$0.36 \pm 0.06$	122.8	1911	97.6	E512	12.62	1.27	−19.4
53	00:24:43.8	−72:07:23	11.62	$0.43 \pm 0.06$	127.7	1940	96.4	E620	12.00	1.59	−24.3

<sup>a</sup>Identification number from Tucholke 1992.

<sup>b</sup>Membership probability from Tucholke 1992.

<sup>c</sup>Identification number from Chun & Freeman 1978.

<sup>d</sup>Also listed as star 1222, with mp=0.

TABLE 2  
VISUAL POLARIZATIONS FOR STARS BETWEEN 4 AND 20 ARCMIN FROM THE 47 TUC NUCLEUS

L <sup>a</sup>	X "	Y "	$P_V$ %	$\theta_V$ °
1421	-190.0	-1060.0	$0.53 \pm 0.05$	101.4
2620	-555.9	-167.2	$0.43 \pm 0.05$	123.7
2705	-492.0	-73.8	$0.50 \pm 0.07$	132.3
2758	-423.1	-373.9	$0.42 \pm 0.04$	112.5
3708	-546.1	64.0	$0.39 \pm 0.05$	110.4
3730	-418.2	167.4	$0.44 \pm 0.05$	121.4
3736	-433.0	196.9	$0.44 \pm 0.06$	118.1
4715	-275.5	260.8	$0.41 \pm 0.04$	121.3
4728	50.0	541.3	$0.48 \pm 0.05$	111.5
4729	50.0	492.1	$0.37 \pm 0.06$	117.9
5312	806.9	885.7	$0.47 \pm 0.06$	118.0
5529	561.0	659.4	$0.46 \pm 0.05$	114.7
5622	226.3	551.1	$0.40 \pm 0.05$	104.9
8756	255.8	-295.2	$0.28 \pm 0.07$	121.6

<sup>a</sup>Identification number from Lee 1977

TABLE 3  
VISUAL POLARIZATIONS FOR VARIABLE STARS IN 47 TUC

Star <sup>a</sup>	$P_V$ %	$\theta_V$ %	$U$ %	$Q$ %
V1	$0.36 \pm 0.06$	99.0	-0.11	-0.34
V2	$0.06 \pm 0.05$	45.0	0.06	0.00
V3	$0.42 \pm 0.05$	105.1	-0.21	-0.36
V4	$0.47 \pm 0.08$	130.7	-0.46	-0.07
V4	$0.23 \pm 0.04$	52.6	0.22	-0.06
V6	$0.36 \pm 0.06$	135.8	-0.36	0.01
V8	$0.47 \pm 0.04$	1.8	0.03	0.47
V10	$0.31 \pm 0.04$	120.5	-0.27	-0.15
V11	$0.47 \pm 0.06$	135.6	-0.47	0.01
V13	$2.37 \pm 0.10$	123.9	-2.20	-0.90

<sup>a</sup>Identification from Sawyer-Hogg 1973

TABLE 4  
VISUAL POLARIZATION FOR THE BRIGHT-STAR-FREE REGIONS IN THE FIELD OF 47 TUC

N	R.A. (J2000) hs : min : s	Dec (J2000) ° : ' : "	$V_{17''}$ mag	$P_V$ %	$\theta_V$ °	P.A. °
1	00:24:01.84	-72:07:01.8	12.78	$0.35 \pm 0.06$	119.5	188.4
2	00:23:52.40	-72:06:31.0	11.78	$0.36 \pm 0.04$	123.5	212.5
3	00:23:43.94	-72:05:41.3	12.23	$0.38 \pm 0.05$	120.7	244.6
4	00:23:44.13	-72:05:11.8	11.89	$0.35 \pm 0.04$	125.0	259.3
5	00:23:44.23	-72:04:23.8	11.67	$0.35 \pm 0.04$	125.8	286.1
6	00:23:49.56	-72:03:52.4	12.03	$0.36 \pm 0.04$	126.0	308.6
7	00:23:55.85	-72:03:23.4	11.99	$0.43 \pm 0.04$	123.2	331.2
8	00:24:06.92	-72:03:15.0	11.83	$0.37 \pm 0.03$	122.1	2.6
9	00:24:18.85	-72:03:16.7	11.67	$0.35 \pm 0.04$	124.2	31.8
10	00:24:17.14	-72:03:40.6	11.86	$0.37 \pm 0.04$	124.8	53.5
11	00:24:30.56	-72:04:43.9	11.49	$0.39 \pm 0.03$	122.0	85.4
12	00:24:27.96	-72:05:38.0	12.72	$0.40 \pm 0.06$	122.4	113.8
13	00:24:22.37	-72:06:10.7	12.39	$0.39 \pm 0.05$	126.7	135.8
14	00:24:16.61	-72:06:46.5	12.41	$0.37 \pm 0.06$	120.3	156.5

TABLE 5  
UBVRI POLARIZATIONS FOR THE NUCLEUS OF 47 TUC

Filter	$\lambda$ nm	$P_\lambda$ %	$\theta_\lambda$ °
<i>U</i> (17'')	360	$0.44 \pm 0.11$	$127.4 \pm 2.5$
<i>U</i> (33'')	360	$0.72 \pm 0.06$	$118.6 \pm 2.5$
<i>U</i> (45'')	360	$0.48 \pm 0.06$	$116.8 \pm 2.0$
<i>B</i>	430	$0.46 \pm 0.02$	$125.6 \pm 1.0$
<i>V</i>	550	$0.36 \pm 0.01$	$124.5 \pm 0.5$
<i>R</i>	630	$0.33 \pm 0.01$	$124.4 \pm 0.5$
<i>I</i>	780	$0.29 \pm 0.03$	$123.8 \pm 1.5$